POLITECNICO DI TORINO
Repository ISTITUZIONALE

Enhancing electric vehicle battery performance and safety through simulation and testing of key electrical components

Original
Enhancing electric vehicle battery performance and safety through simulation and testing of key electrical components / Farooq, U., Galfre, G., Bertana, V., Ferrero, S., Costa, L., Bigaran, S., Costa, L., Scaltrito, L.. - In: JOURNAL OF ENERGY STORAGE. - ISSN 2352-152X. - 147:(2026), pp. 1-9. [10.1016/j.est.2025.120036]

Availability:
This version is available at: 11583/3006263 since: 2026-01-02T19:27:26Z

Publisher:
Elsevier

Published
DOI:10.1016/j.est.2025.120036

Terms of use:

This article is made available under terms and conditions as specified in the corresponding bibliographic description in the repository

Publisher copyright

(Article begins on next page)

20 November 2026

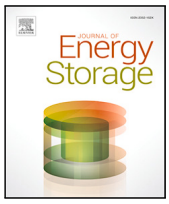
Journal of Energy Storage 147 (2026) 120036



Contents lists available at ScienceDirect

Journal of Energy Storage

journal homepage: www.elsevier.com/locate/est



Research papers

Enhancing electric vehicle battery performance and safety through simulation and testing of key electrical components

Umar Farooq [a,b,c,*], Giulio Galfre [a], Valentina Bertana [a], Sergio Ferrero [a], Luca Costa [c], Simone Bigaran [c], Luigi Costa [c], Luciano Scaltrito [a]

[a] Chilab-ITEM laboratory, Department of Applied Science and Technology (DISAT), Politecnico di Torino, Corso Duca degli Abruzzi 24, Turin, 10129, Italy
[b] Department of Science and Technology Innovation (DISIT), Università del Piemonte Orientale, Viale Teresa Michel 11, Alessandria, 15121, Italy
[c] R&D Innovation Department, MISTA S.p.A, Via Roma 79/A, Cortiglione–Asti, 14040, Italy

ARTICLE INFO

Keywords:
Battery packs
Copper busbars
Digital twin
Electric vehicles
Laser welding
Multi-physics simulation

ABSTRACT

The development of electric vehicles (EVs) depends on effective and secure battery systems in high current scenarios like fast charging and acceleration. The effects of these incidents are excessive heating, mechanical stress and failure of electrical connections. This study presents a prototype of a multi-physics Digital Twin that is a model of electromagnetic, thermal, and structural environments that evaluates the functionality of copper busbars operating at EV operating current levels (100–500 A). The framework will consist of a combination of cross-domain corroboration as simulations with the use of finite-elements and experimental testing. The measurements indicate steady operation up to 200 A, small voltage drops (0.009–0.047 V), contact resistances (12.4–18.7 μΩ), and magnetic emissions (8–40 mT), all within the IEC 60269-1, IEC 61439-1 and CISPR 25 limits. Localized heating (273 °C) and deformation (>1 mm) at 500 A transient loads are characteristic of critical conditions, leading to design changes in the form of increased cross-sectional thickness, integral cooling, and laminated structures. The paper presents an experimentally evaluated prototype of a Digital Twin which is a bridge between simulation and physical experiment and can be used as a predictive instrument in safer and more dependable busbar design in future EV battery systems.

1. Introduction

The global transition towards electric mobility is attributed to growing environmental concerns, thereby driving advancements in battery technology. However, the performance and safety of electric vehicles (EVs) remain critically dependent on the reliability of their battery packs [1,2]. Within these battery packs, busbars are crucial components for distributing high currents between cells and modules. Their failure under extreme operational loads, such as during fast charging or acceleration, can lead to increased resistance, localized overheating, and even thermal runaway, thus presenting a significant barrier to reliability and safety [3–7].

The selection of the material composition (e.g. aluminum, copper) of busbars and their joining methods (e.g., ultrasonic welding, laser welding, etc.) are critical for optimizing performance, guaranteeing durability, and preventing localized hotspots that could lead to premature degradation or thermal runaway [8–11]. Consequently, the deployment of high-performance busbars is vital to extend the lifetime, safety, and efficiency of electric vehicle battery systems. Copper has excellent electrical conductivity, low resistive losses and is also quite corrosion resistant, which guarantees long term reliability with harsh EV battery operating conditions [12–14]. The ductility of the metal allows for design flexibility when using in high current applications [15].

Traditional prototyping and testing methodologies, though foundational, involve significant time and cost limitations, which restrain comprehensive assessment of multi-physical interactions under operational conditions [16,17]. To resolve such problems, the Digital Twin (DT) approach is being recognized as an important innovation in the context of Industry 4.0 by bridging the gap between virtual models and physical systems [18–25]. For instance, cell-to-cell heat transfer and interconnect resistance significantly influence current distribution and anode potential in Li-ion modules, potentially leading to lithium plating during fast charging [26,27]. Thermal topology optimization methods for laminated busbars can minimize copper use while maintaining temperature limits, improving cost-performance ratios [28,29].

* Corresponding author at: Chilab-ITEM laboratory, Department of Applied Science and Technology (DISAT), Politecnico di Torino, Corso Duca degli Abruzzi 24, Turin, 10129, Italy.
E-mail addresses: umar.farooq@polito.it, umarfarooqist01@gmail.com (U. Farooq).

https://doi.org/10.1016/j.est.2025.120036
Received 1 September 2025; Received in revised form 14 November 2025; Accepted 19 December 2025
2352-152X/© 2025 The Authors. Published by Elsevier Ltd. This is an open access article under the CC BY license (http://creativecommons.org/licenses/by/4.0/).

Even though there is extensive research on busbars, all the literature is mostly based on isolated studies of electrical, thermal, or mechanical properties [15,30], and thus the literature does not acknowledge the interaction effect on busbars in the context of the actual electric vehicle. This fragmented approach to analysis can result in less than optimum designs, or heavy over-engineering, but more importantly, unexpected failures due to multiple dynamic multi-physical loads. In order to help mitigate this problem, the current research explores an integrated multi-physics DT prototype. Virtual replica of the physical busbar was created and simulation was performed to analyze the complex interactions between the electromagnetism, thermodynamics and structural mechanics under realistic operating conditions. It is important to note that, even though the current study focuses on the busbar element, the current profiles (100–500 A) used in the testing process essentially represent current profiles in modern high-capacity NMC/Gr (lithium-nickel-manganese-cobalt-oxide/graphite) Li-ion battery packs utilized in electric vehicles.

This study makes two main contributions: (1) The proposed coupled electro-thermal-mechanical model to quantify nonlinear interactions, e.g. Joule heating — caused deformation. (2) The developed DT prototype supported by experimental testing serve to connect simulations and physical measurements and provide capabilities for prospective real-time optimization of the design of the busbars. The research offers a scientific contribution in establishing a busbar electro-thermal performance/deformation-driven reliability limit multi-physics coupling. This provides a predictive modeling method that can predict degradation of performance before failure occurs, and an improved theoretical understanding of the coupled field behavior in current carrying conductors. The work also explains how components of the current distribution affect the efficiency, life and safety of energy-storage systems used in electric vehicles.

2. Materials and methods

2.1. Busbar materials and selection justification

Copper busbars (supplied by Mista S.p.A, Italia) were selected in the current study. Three types of copper busbar resources were tested, in order to represent important electrical paths in EV battery systems:

- Type I (large): 216 mm × 14 mm × mm (large) Laser welded busbars for primary current distribution
- Type II (medium): 108 mm × 14 mm × 3 mm Rigid busbars for inter-module connection
- Type III (small) 83 mm × 64 mm × 3 mm, for inter-cell links (subtypes A–C by geometry)

Dimensions and surface finishes were in accordance with IEC 61439-1 making them industrially relevant.

2.2. Laser welding process

In case of laser welded copper busbars (Type I), the laser welding process was carried out using a high-precision laser welding machine (FL 8000–ARM 100/290) according to the BS EN ISO 13919-1-2019 standard. Selective laser parameters, such as power (8 kW), focus position (0 mm), and speed (50 mm/s), were used to acquire the optimum possible weld quality. The welding process was carried out carefully to ensure uniformity and reliability in the welded joints.

Table 1
COMSOL® interfaces, governing equations, and boundary conditions used in the multi-physics Digital Twin prototype.

COMSOL Interfaces	Governing Equations	Assumptions and Boundary Conditions
AC/DC	(i) $\nabla \times \mathbf{H} = \mathbf{J}$ (ii) $\mathbf{J} = \sigma \mathbf{E}$ (iii) $Q = \mathbf{J} \cdot \mathbf{E}$	• Current density (J_0) from experimental range • Zero initial electric potential • No external magnetic field • Known σ
Heat Transfer	(iv) $\rho C_p \frac{\partial T}{\partial t} = \nabla \cdot (k \nabla T) + Q$	• $T_0 = T_{ref} = 22\,^{\circ}\mathrm{C}$ • Known k, C_p • Joule heating coupling
Solid Mechanics	(v) $\nabla \cdot \mathbf{S} + \mathbf{F}_v = \mathbf{0}$ (vi) $\epsilon = \epsilon_{el} + \alpha \Delta T \mathbf{I}$	• Fixed bolted regions • Known E, ν • Thermal expansion coupling

2.3. Governing equations and simulation framework

A multi-physics simulation framework was developed using the COMSOL® Multiphysics 6.3 simulation software package for coupling the electromagnetic, thermal and structural domains to analyze the behavior of copper busbars when operating at high currents. The model combines four physics interfaces — Magnetic and Electric Fields, Heat Transfer in Solids, Solid Mechanics and Electromagnetic Heating/ Thermal Expansion nodes, as the DT prototype of the busbar. The busbar geometry was imported via the STEP file, surrounded by an air box for magnetic field modeling. Table 1 shows the details of governing equations. The evaluation of important phenomena such as voltage drop, magnetic flux density, Joule heating and thermally induced mechanical strain was obtained under realistic boundary conditions.

Boundary conditions were fixed bolt constraints, ambient temperature 22 °C and applied current densities for 100–500 A. Material parameters σ, k, ρ, C_p, ϵ, and α were taken from the built-in copper and air material data in COMSOL® Multiphysics 6.3.

2.4. Experimental characterization

2.4.1. Mechanical testing

Performance evaluation of laser-welded Cu busbars (Type I) was carried out using different mechanical tests, including 3-point bend tests, bending tests, and torsional tests following the ISO 7438 (bend test) and ASTM E143 (torsion testing) protocols. Each test was repeated three times per condition (n = 3), and mean ± standard deviation values are reported. 3-point bend tests, and bending tests were performed using a Galdabini Universal Testing Machine (UTM) with a load cell of 30 kN and at testing speed of 25 mm/min. The bending test was performed by applying force using a round stainless steel pin on the specimen clamped firmly with the metallic clamps of the machine. Torsion tests were performed on Instron Torsional Test Equipment. Further, torsional forces and associated properties were evaluated to examine the response of the welded region to twisting forces.

2.4.2. Electrical and magnetic characterization

The magnetic flux density near small copper busbars (Type III) was measured using an ACS37612 Hall-effect current sensor (Allegro Microsystems), selected for its contactless current measurement capability as shown in Fig. 1. The test was carried out at 40 A discharge current with a 3.3 V sensor supply. Sensor placement (e.g., over holes or narrowed sections) was optimized through simulations and validated experimentally as discussed in Section 3.3. Measurements were repeated to verify consistency (variation below ± 3%), which confirms the reliability of the sensor.

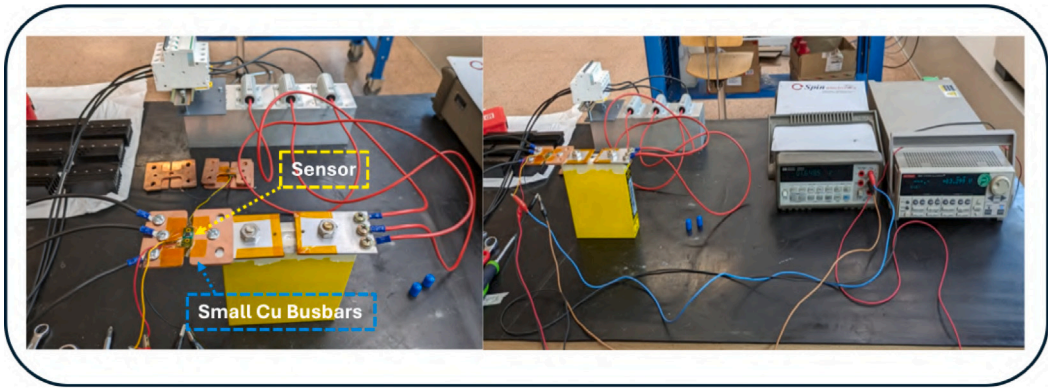


Fig. 1. Magnetic flux density measurement setup using ACS37612 Hall-effect sensor on small copper busbars (Type III). The sensor captured near-field flux at 40 A for Digital Twin corroboration.

Table 2
Characterization matrix summarizing simulation and experimental methods for large (Type I), medium (Type II), and small (Type III) copper busbars.

Busbar Type	Simulation	Experimental
Type I	Electrical Performance	3-point Bend Test
	Thermal Endurance	Torsion Test
	Electromagnetic–Compatibility	Edge Bending Test
		Optical Microscopy
Type II	–	Contact Resistance
Type III	Electromagnetic–Compatibility	Electromagnetic–Compatibility

2.4.3. Microscopic analysis

Welded region of laser welded busbars (Type I) were analyzed using an Olympus DSX 1000 microscope. Cross-sections were prepared by sequential grinding with emery paper (grit sizes: 120, 500, 1000, 2000) and etched with $FeCl_3$ solution (10% w/v, 25 °C, 10 min) to enhance grain boundary visibility. Images were taken in both bright-field (BF) and differential interference contrast (DIC) modes of the microscope to enhance the visibility of the area of interest, i.e. welded regions in large busbars (Type I).

2.4.4. Contact resistance measurement

The contact resistance of medium copper busbars (Type II) was measured using both two-probe and four-probe techniques, in accordance with IEC 60269-1 guidelines. Busbars were bolted to a silver busbar using a torque of 3.2 Nm. A DC current source (10 A, two-probe) and (1 A, four-probe) provided current for resistance measurements. Results are discussed in Section 3.2. Each measurement of the resistance was repeated 3 times and the values reported represent the average (mean). Measurement error was not more than 0.2 μΩ.

Evaluation of Cu busbars through various simulations using COMSOL® Multiphysics and experimental characterizations using different equipment are summarized in Table 2.

The combination of experimental and simulation framework allows qualitative and quantitative validation of the developed DT prototype. This integration means that each of the physical parameters measured experimentally (magnetic flux, deformation, resistance) has a direct relationship with its simulated counterpart for cross verification. Each of the experimental tests was repeated three times and under the same conditions to ensure reproducibility. Mean values and standard deviations of all measurements were calculated and coefficients of variation were calculated and were less than 8%. This low variability is an indication of the repeatability and stability of the measurement procedures, which provides adequate confidence level in the experimental data used in supporting the trends in the simulation.

3. Results and discussion

3.1. Type I: Large laser-welded busbars - Digital twin and experimental study

3.1.1. Multi-physics simulation predictions

In alignment with practical EV battery operational profiles, the simulations were carried out under operational current values (100–500 A) using COMSOL® Multiphysics. The selected current range, 100 A, 150 A, and 200 A, represents typical pack-level continuous operation, while 500 A accounts for peak transient loads observed during initial vehicle startup or high acceleration events. In the simulations, current was applied to one terminal/end with the other grounded, to study the behavior of the Cu busbar for electric potential, magnetic fields, temperature changes, and structural displacement under these conditions.

Static simulation of the busbar showed stable electric potential distribution (Fig. 2a) with voltage drops increasing linearly with current: 0.00948 V (100 A), 0.0142 V (150 A), 0.019 V (200 A), and 0.0474 V (500 A). All values remain well within the safety limits prescribed by the IEC 61238-1 standard for power components. While the 500 A startup surge causes a larger drop (0.0474 V), it remains acceptable for short durations; however, for frequent high-current events, designs with a larger cross-sectional area could be considered to further minimize resistive losses. Detailed maps of voltage drop at 100 A, 150 A, 200 A and 500 A are given in supplementary material (Figures S1–S4) for reference.

Fig. 2b shows the magnetic flux densities values due to operational currents (A). Peak magnetic flux densities were observed as 8 mT (100 A), 12 mT (150 A), 16 mT (200 A), and 40 mT (500 A). These values scale proportionally to the current according to Ampère's law. Moreover, the symmetric flux pattern verifies the suitability of the geometric design, preventing eddy currents. For typical operational conditions (up to 200 A), the flux density remains well below the regulatory thresholds as per CISPR 25 and ISO 11452 (commonly 30–40 mT for fixed installations).

As shown in Fig. 2c, the temperatures increased from 30 °C to 273 °C during 100 A–500 A. At current value $\leq$ 200 A, the increased temperature across busbar was within safe limits while 500 A led to the formation of localized hot-spots (≈273 °C) near the weld region. The critical temperature of 273 °C at 500 A is significantly higher than the maximum long-term service temperature of common insulating materials and can lead to a high risk of material degradation, copper annealing and possible connection lines. This outcome identifies the need for mitigation strategies for applications that include transient peak loads are: (1) using active cooling channels along beneath the busbar; (2) using thermal conductive interface materials to redirect heat to the cold plate of the battery pack; or (3) making laminated

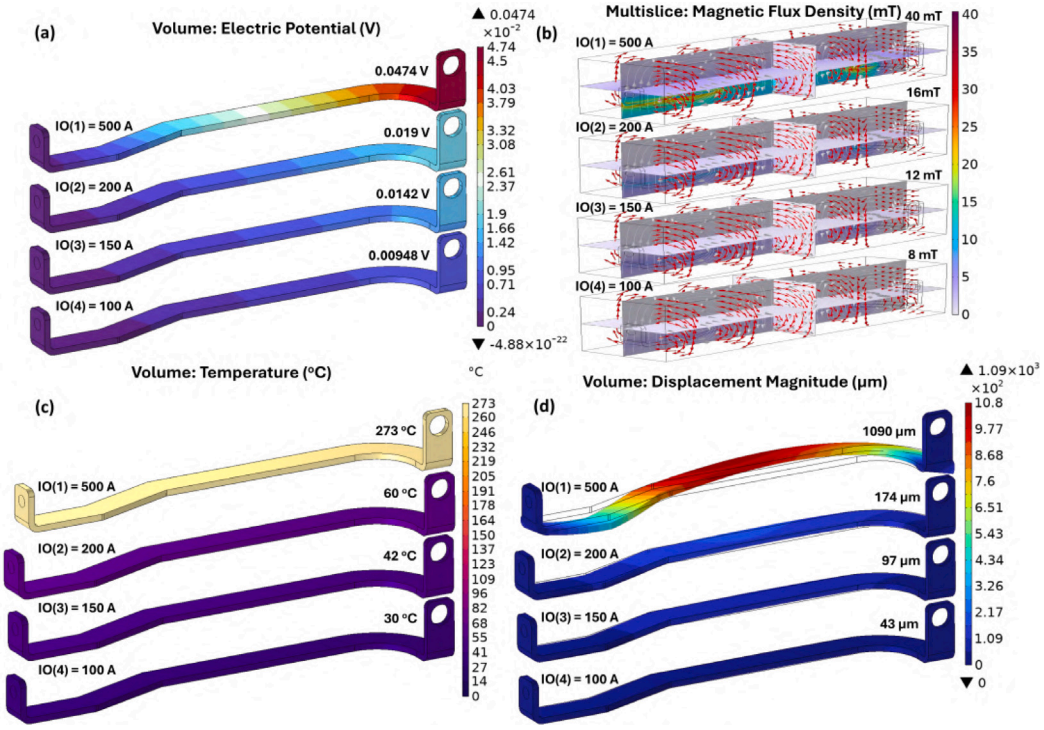


Fig. 2. Multi-physics simulation of large laser-welded busbar (Type I): (a) electric potential, (b) magnetic flux, (c) temperature field, (d) thermal deformation. Results form the Digital Twin prototype framework.

busbar structures. Corresponding simulations for temperature field under different loads of current are shown in the supplementary material (Figures S5–S8), which reveals the localized heating trend close to the welded joints.

The thermomechanical simulations (Fig. 2d) evaluated busbar reliability under combined thermal-electrical loads, predicting thermal expansion and deformation patterns. Associated mechanical deformation due to thermal expansion was predicted as 43 µm at 100 A, 97 µm at 150 A, 174 µm at 200 A, and 1090 µm at 500 A. At lower currents, the structure exhibits minimal deflection, indicating stable thermomechanical behavior. However, at 500 A, the large deformation necessitates design revisions for mechanical reinforcements or thermal expansion joints, especially in weld-sensitive areas.

While the simulated and experimental tests have been concerned with different domains of responses, they involve the same physical system and the same material behavior. The simulating part is able to predict the electrical, thermal and mechanical response facing high current loading but experiments capture the actual structural, magnetic and resistive features of the same copper busbars. The trends seen and the consistency of findings – such as localization of heating zones corresponding to weaker zones in the weld, and the predicted magnetic flux distributions in line with measurements of the sensors – are cross-domain corroborations. This way it is possible to ensure that the DT framework will have the same effort to approximate the realism of the performance envelope of the busbars even though individual parameters may not have been directly measured in the same boundary conditions. High resolution field distributions in support of these findings are also included in the supplementary material.

3.1.2. Experimental evaluation and correlation

Fig. 3 shows the specimen during 3-point bend test, and corresponding results, respectively. The 3-point bend tests were conducted on both the flat and welded regions of the busbar to evaluate the maximum force and yield force endured by laser welded busbar by applying force through loading span on the specimen supported by two support spans of a fixture. 3-point bend test results of laser welded copper busbars indicated that the maximum force (kN) and yield force (kN) endured by the flat region of copper busbar without weld were higher compared to the laser welded region of the copper busbar.

Particularly, the flat region showed a maximum force of 2.43 ± 0.05 kN and the yield force of 1.60 ± 0.02 kN, while the welded region of the copper busbar exhibited a maximum force of 1.53 ± 0.11 kN and the associated yield force as 0.78 ± 0.05 kN. These results signify that the welded region of the copper busbar, although strong, is slightly less resistant to the bending forces compared to the bulk material. This means a loss of mechanical strength of about 37% for the maximum force and 51% for the yield force at the welded joint. This degradation is directly related to the changes in the microstructure of the weld zone (e.g. grain coarsening, micro-void formation, etc.) as discussed later.

The primary objective of the bending test (Fig. 4) was to measure the force required to bend the laser-welded region to understand the flexibility of the welded region. The bending test revealed that the force required to bend the laser welded region was 362 ± 50 N, indicating that the laser-welded joint maintained sufficient strength to resist the bending force, preserving the mechanical integrity of the copper busbars, and ensuring the overall reliability of battery systems. Moreover, by further improving the quality of the weld, it is possible to improve the strength of the Cu busbars thereby increasing their reliability and performance in high-demand applications, such as electric vehicles and renewable energy systems. In addition, the enhancement in weld quality could facilitate significant reduction in maintenance costs as well as increasing the lifespan of critical components.

Fig. 5 illustrates the laser welded Cu busbar under torsion test providing rotational force (N) endured by the Cu busbar and the resultant associated properties calculated by selecting maximum load value acquired during torsional testing. Load (N) denotes the torsional force applied, while displacement (mm) measures angular twist. Evaluating mechanical performance of the laser-welded Cu busbar region under torsional load of 1200 N, the associated key parameters were calculated, including the torsional constant (J) equal to 144 mm^4, twist angle (β) equal to 20.1°, torsional stiffness (C) equal to 33.6 Nm/rad, and torque (T) achieved equal to 675 Nm. Results show that the

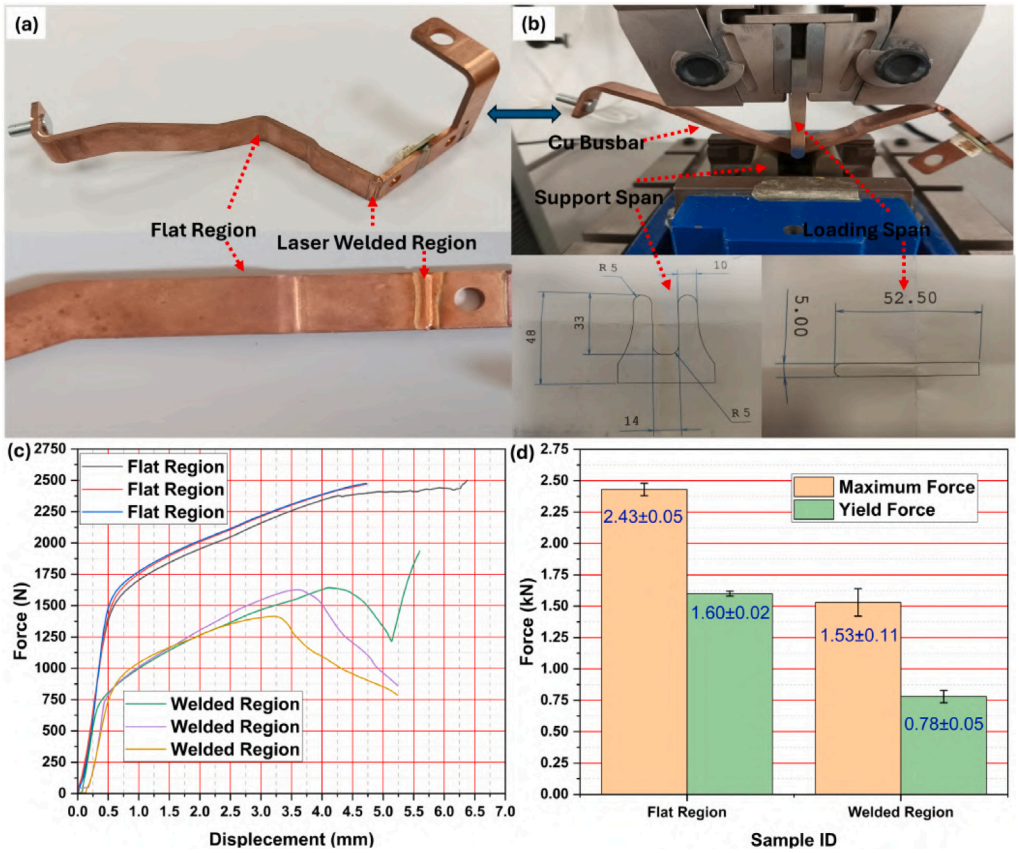


Fig. 3. Three-point bend test of laser-welded copper busbar: (a–b) setup, (c–d) force–displacement results. Welded zones show reduced strength compared to bulk copper.

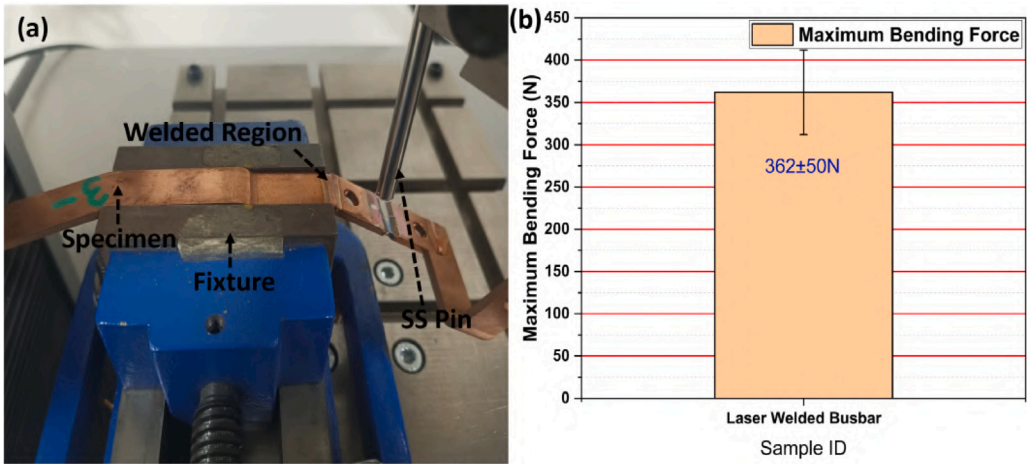


Fig. 4. Bending test of welded busbar: (a) deformation during loading, (b) mean bending force (n = 3, ±1 SD). Welded region retains sufficient flexibility for EV applications.

measured torsional stiffness (33.6 Nm/ rad) and acquired torque value (675 Nm) signify the mechanical endurance of the welded joint for high loads in EV cycles.

Optical microscopy analysis of the welded region showed a distinct difference in grain structure compared to the bulk material. The fusion zone, i.e., welded region in laser-welded copper busbar as shown in Fig. 6, contains coarse grains, which contributed to reduced mechanical strength compared to the base metal. However, as suggested by some researchers, grain refinement techniques, such as double-pass welding, can disrupt the growth of these coarse grains, and ultimately could lead to improvement in the mechanical properties of the welded region [31].

In addition, micro-voids present in the welded region as visible in Fig. 6, could also be substantial contributors towards mechanical and electrical performance degradation. These defects can lead to crack formation, which further compromising the laser weld integrity.

3.2. *Type II: Medium rigid busbars - Contact resistance performance*

The contact resistance measurements of Cu busbars showed values within the acceptable range (< 20 μΩ) in accordance with IEC 60269-1 for the final application. The two-probe test of Cu busbars (Fig. 7)

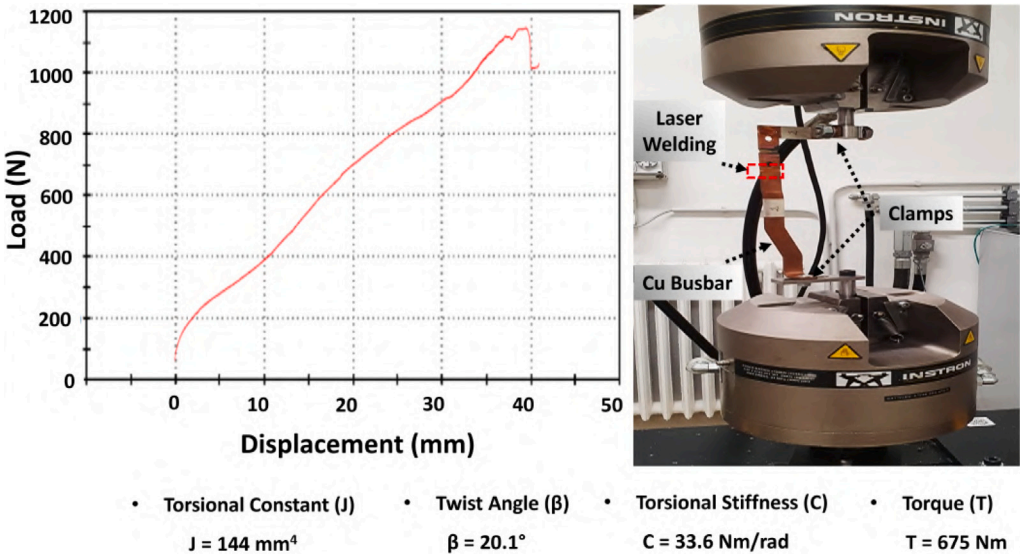


Fig. 5. Torsion test of laser-welded busbar showing rotational load–displacement response. Measured torque capacity (675 Nm) confirms strong joint integrity.

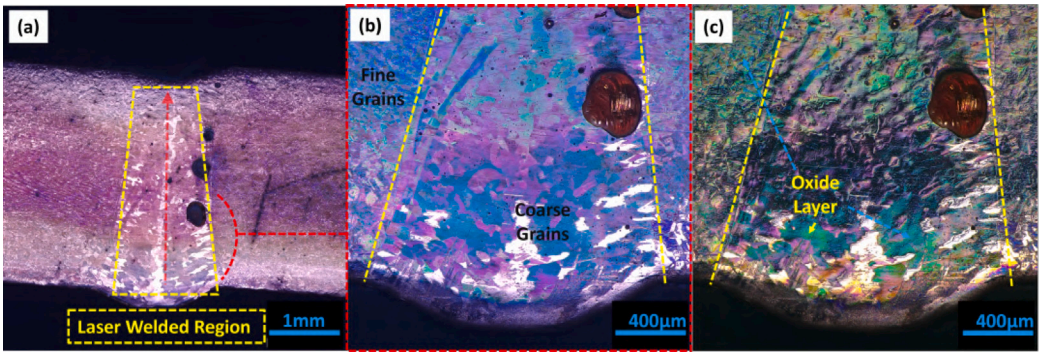


Fig. 6. Optical micrographs of laser-welded region: (a–b) bright-field, (c) DIC mode. Coarse grains and voids explain the local strength reduction in welded zones.

performed at the value of current equal to 10 A showed a contact resistance of 14.7 μΩ - 18.7 μΩ, while the four-probe test (Fig. 7) performed at the value of current equal to 1 A for the same specimens showed contact resistance values 12.4 μΩ - 18.0 μΩ. This indicates that the oxide layer formed on the surface of the busbars did not significantly impact their electrical functionality. The oxide layer, although affecting the aesthetic appearance, acted as a passivating film that protected the underlying copper from further oxidation and corrosion. Therefore, thin oxide layers on copper surfaces can enhance long-term reliability without compromising significantly electrical performance [32,33].

3.3. Type III: Small busbars - Geometric influence on magnetic flux

Magnetic flux densities (mT) were simulated and experimentally measured using current value 40 A for three distinct small copper busbar configurations (Fig. 8, Table 3) labeled as A, B, and C, respectively. Simulated and measured flux density at 1.6 mm from center showed excellent agreement (0.40 mT (simulated) vs 0.426 mT (measured) for Sample A - Samples B and C showed 1.85 and 2.1 mT respectively still within ICNIRP 2010 and UNECE R10 (10 mT limit). The findings validate the significance of geometry in the distribution of the field and support the simulation method. The observed difference in the magnetic flux values of B and C may attribute to the edge effects and current crowding phenomena due to thin cross-section compared to busbar A. Magnetic flux distributions for all Type III geometries (A–C) and details on sensor attachment as well as streamline distributions are shown in supplementary material (Figures S9–S11).

Table 3
Comparison of simulated and experimentally evaluated magnetic-flux distributions for small busbars (Type III) at 40 A current at a distance of 1.6 mm from the central point.

Sample ID	Variation (mv)	Sensitivity (mV/A)	Magnetic Field (mT)–Sensor	Magnetic Field (mT)–Simulation
A	42.6	1.065	0.426	0.40
B	76.5	1.913	0.765	1.85
C	69	1.725	0.69	2.1

3.4. Performance benchmarking and designing implications

The results for performance measurements from our study are in agreement with the latest results in the literature on high-current interconnects. The measured contact resistance of 12.4–18.7 μΩ is on the low end of 15–25 μΩ for ultrasonic Al–Cu joints [11] and performance of advanced joining-by-forming processes [10]. The important increase in the terminal temperature found at 500 A ($\nabla T \approx 248$ °C) is in agreement with literature, for example Mypati et al. [7] recorded high joule heating in busbars of similar designs, while Kalkan [6] covered the importance of thermal management being an integral part of the solution. Deformation larger than 1 mm at 500 A signifies the importance of electro-thermo-mechanical coupling as also observed by Werling et al. [15]. Similar approach for EV components was adopted by Ling et al. [23] for full vehicles systems and Muslu et al. [22] for power electronics. Validation of our magnetic flux simulations

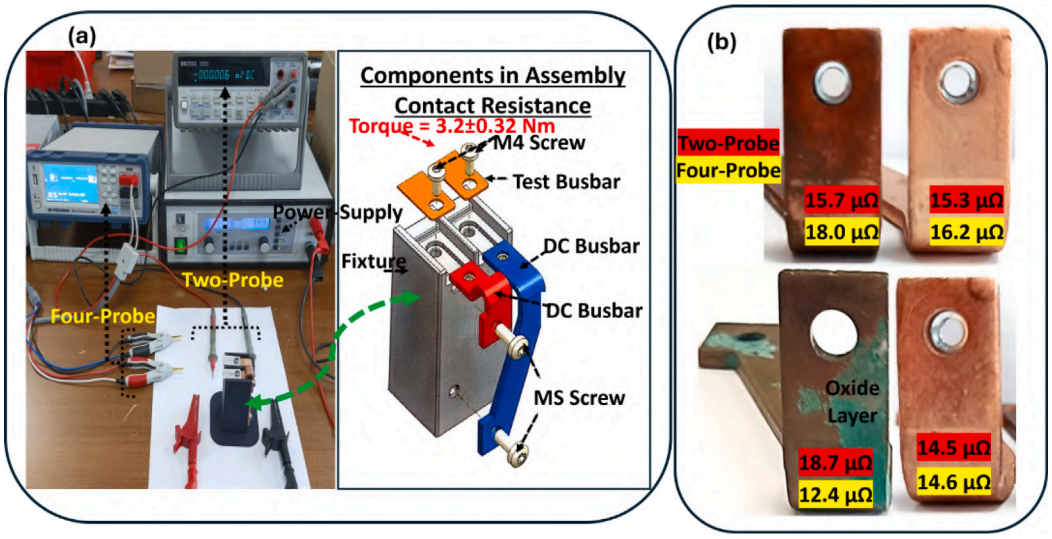


Fig. 7. Contact-resistance measurements for medium busbars (Type II): (a) test setup, (b) results. All values (12.4–18.7 μΩ) meet IEC 60269-1 thresholds.

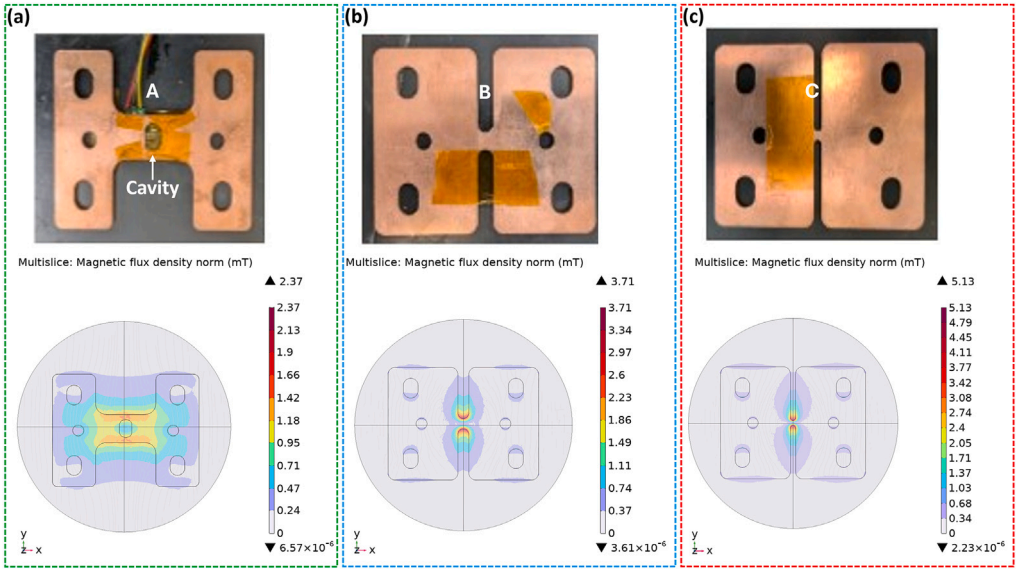


Fig. 8. Simulated magnetic-flux distributions for small busbars (Type III) at 40 A current: (a) Sample A, (b) B, (c) C. Showing current crowding phenomena in the mid region of busbars.

with sensor information enhances confidence in the reliability of the developed framework in the context of EMI compliance as per CISPR 25 and UNECE R10. Moreover, the mechanical strength retention of about 65% in welded areas is a vital finding in the research area of integrity of laser welded joints as also studied by Kumar et al. [9] and Ramachandran et al. [34] who examined the impact of the microstructure on performance. Our 40 A measurements of the near-field magnetic flux (with probe 1.6 mm distance) are consistent (within order) with literature on busbar geometry/inductance and magnetic flux control, including literature on the effects of aperture position, terminal layout and lamination in reducing B and stray inductance as explained in city-bus field surveys (larger local values in closer standoff, as in ours) [35]. This complete comparison not only confirms the validity of our experimental and simulation results but also specifies our integrated methodology of Digital Twin as a powerful tool to solve the multifaceted and multiphysical design issues facing the EV battery system in modern EVs. The concluding section summarizes these implications as well as future extensions of the developed Digital Twin prototype.

4. Conclusion

Our study have developed a multi-physics DT prototype for the design and evaluation of copper busbars in EV battery packs. The framework couples electromagnetic domain, thermal and mechanical domains in order to capture the inter-dependence of the current distribution, Joules heating and deformation. The simulations, which have been supported by mechanical and magnetic and contact resistance experiments, provide support from several areas cross-domain corroboration of the predicted trends as well as verification of the physical realism of the model.

Key results indicate that copper busbars continue to operate safely up to 200 A that complies with IEC 61238-1 and CISPR 25 requirements. At higher transients longer term currents e.g. 500 A or so are exceeded localized heating and expansion occurs and design measures such as thick cross-section or embedded cooling channels or laminated structures will be required. Laser welded joints contain approximately 65% of the strength of the base metal thereby marking areas of welds as mechanically sensitive areas.

The contribution of the study is scientific as we quantify the coupled electro-thermo-mechanical response in a validated implementation environment and highlight how this approach can be used to predict thresholds related to failure before physical testing. Rather than being a fully-data linked Digital Twin the current model is a high fidelity virtual prototype and can be evolved to a real-time twin once integrated with operational sensing data.

Future work will involve time-dependent thermal-cycling and fatigue analyses, environmental effects (vibration and humidity), as well as the inclusion of real-time information for predictive health monitoring of busbar systems at the battery pack level. The proposed work bridges the numerical modeling and experimental testing and thus offer a scalable methodology for future electric vehicles energy storage research and industrial design optimization.

5. Nomenclature

Symbol	Description
Roman Symbols	
$\mathbf{B}$	Magnetic flux density (T)
C	Torsional stiffness (Nm/rad)
C_p	Specific heat capacity (J kg^{-1} K^{-1})
$\mathbf{E}$	Electric field (V m^{-1})
$\mathbf{F}_v$	Volume force (N m^{-3})
I, I_0	Current, Applied current (A)
$\mathbf{J}$, J_0	Current density, Applied current density (A m^{-2})
k	Thermal conductivity (W m^{-1} K^{-1})
Q	Joule heating source term (W m^{-3})
$\mathbf{S}$	Stress tensor (Pa)
T	Temperature (°C, K)
T_{ref}	Reference temperature (°C, K)
V	Electric potential (V)
Greek Symbols	
α	Thermal expansion coefficient (K^{-1})
β	Twist angle (degrees, rad)
ϵ	Total strain tensor
ϵ_{el}	Elastic strain tensor
μ_0	Permeability of free space (H m^{-1})
ν	Poisson's ratio
ρ	Density (kg m^{-3})
σ	Electrical conductivity (S m^{-1})
ΔT	Temperature change (K)
Abbreviations	
CISPR	Comité International Spécial des Perturbations Radioélectriques
DT	Digital Twin
EMC	Electromagnetic Compatibility
EMI	Electromagnetic Interference
EV	Electric Vehicle
FEM	Finite Element Method
IEC	International Electrotechnical Commission
ISO	International Organization for Standardization
Units	
kN	Kilonewton
mT	Millitesla
Nm/rad	Newton meter per radian
μΩ	Microohm

CRediT authorship contribution statement

Umar Farooq: Writing – original draft, Software, Methodology, Formal analysis, Data curation, Conceptualization. **Giulio Galfre:** Software, Methodology, Data curation, Conceptualization. **Valentina Bertana:** Writing – review & editing, Visualization, Validation, Resources, Project administration. **Sergio Ferrero:** Writing – review & editing, Visualization, Data curation, Conceptualization. **Luca Costa:** Software, Resources, Data curation, Conceptualization. **Simone Bigaran:** Validation, Supervision, Resources, Data curation, Conceptualization. **Luigi Costa:** Visualization, Supervision, Resources. **Luciano Scaltrito:** Writing – review & editing, Validation, Supervision, Resources, Project administration, Methodology, Investigation, Funding acquisition, Conceptualization.

Declaration of Generative AI and AI-assisted technologies in the writing process

During the preparation of this work the author(s) used Consensus.ai and SCISPACE in order to improve the readability and language of the manuscript. After using this tool/service, the author(s) reviewed and edited the content as needed and take(s) full responsibility for the content of the publication.

Funding

This work received support from the PNRR–NGEU program under MUR – DM 352/2022 and DM118/2023.

Declaration of competing interest

The authors declare that they have no known competing financial interests or personal relationships that could have appeared to influence the work reported in this paper.

Acknowledgments

This publication is part of the project PNRR–NGEU which has received funding from the MUR – DM 352/2022 and DM118/2023. This work contributes to the theme of "Infrastructures for sustainable mobility", and the results will be applied to energy management relating to sustainable mobility, renewable sources, and distributed generation, with a particular focus on the electric mobility sector. The research activity was carried out in collaboration with MISTA S.p.A, Italy, a company specializing in connectors and electrical connections. Moreover, the activities presented in this paper were conducted within the SMIP (Sistemi Microelettronici in Package) project, funded by the Piedmont Region through the SWIch call (Programma regionale FESR 2021/2027).



Appendix A. Supplementary data

Supplementary material related to this article can be found online at https://doi.org/10.1016/j.est.2025.120036.

Data availability

All the data is already available in the manuscript and the supplementary file.

References

[1] M. Despeisse, B. Johansson, J. Bokrantz, G. Braun, A. Chari, X. Chen, Q. Fang, C.A. González Chávez, A. Skoogh, J. Stahre, et al., Battery production systems: state of the art and future developments, in: IFIP International Conference on Advances in Production Management Systems, Springer, 2023, pp. 521–535.

[2] P.J. Paul, P. Anitha, S. Akash, A. Shaju, A. Joy, E.X. Dcoutho, Design and development of triple energy storage system (TESS) for electric vehicle application, in: 2024 Second International Conference on Smart Technologies for Power and Renewable Energy, SPECon, IEEE, 2024, pp. 1–6.

[3] B. Johansson, M. Despeisse, J. Bokrantz, G. Braun, H. Cao, A. Chari, Q. Fang, C.A. González Chávez, A. Skoogh, H. Söderlund, et al., Challenges and opportunities to advance manufacturing research for sustainable battery life cycles, Front. Manuf. Technol. 4 (2024) 1360076.

[4] J. Vijaychandra, Ł. Knypiński, A comprehensive review on challenges and possible solutions of battery management systems in electric vehicles, in: 2024 Progress in Applied Electrical Engineering, PAEE, IEEE, 2024, pp. 1–6.

[5] B. Mayer, M. Schier, H.E. Friedrich, Stand-alone battery thermal management for fast charging of electric two wheelers—integrated busbar cooling, World Electr. Veh. J. 10 (2) (2019) 37.

[6] O. Kalkan, Thermal performance improvement of an air-cooled 18650 NMC battery module: A novel busbar design that acts as a turbulator, J. Energy Storage 88 (2024) 111613.

[7] O. Mypati, T. Anwaar, D. Mitra, S.K. Pal, P. Srirangam, Characterization and modelling of Al and Cu busbar during charging and discharging of Li-ion battery for electric vehicles, Appl. Therm. Eng. 218 (2023) 119239.

[8] P.K. Choudhary, S. Chauhan, R. Chengalvarayan, R.S. Gunti, Study on optimization of ultrasonic welding process parameters of Al-Cu bimetallic busbar for use in battery electric vehicle (EV), in: 2023 IEEE International Transportation Electrification Conference, ITEC-India, IEEE, 2023, pp. 1–10.

[9] N. Kumar, I. Masters, A. Das, In-depth evaluation of laser-welded similar and dissimilar material tab-to-busbar electrical interconnects for electric vehicle battery pack, J. Manuf. Process. 70 (2021) 78–96.

[10] V.B. Gomes, M.M. Kasaei, R.J. Carbas, E.A. Marques, L.F. da Silva, A new joining by forming process for busbar-prismatic cell interconnections in electric vehicle batteries, Int. J. Adv. Manuf. Technol. (2025) 1–28.

[11] A. Das, A. Barai, I. Masters, D. Williams, Comparison of tab-to-busbar ultrasonic joints for electric vehicle Li-ion battery applications, World Electr. Veh. J. 10 (3) (2019) 55.

[12] R.G. Maev, V. Leshchynsky, E. Strumban, M. Pantea, B.J. Robert, T.P. Brackett, Tab-to-busbar interconnects formed by dual flow cold spraying, in: International Thermal Spray Conference, vol. 84536, ASM International, 2023, pp. 597–603.

[13] S.-b. Zhang, F. Nie, J.-p. Cheng, H. Yang, Q. Gao, Optimizing the air flow pattern to improve the performance of the air-cooling lithium-ion battery pack, Appl. Therm. Eng. 236 (2024) 121486.

[14] A. Das, T. Ashwin, A. Barai, Modelling and characterisation of ultrasonic joints for Li-ion batteries to evaluate the impact on electrical resistance and temperature raise, J. Energy Storage 22 (2019) 239–248.

[15] T. Werling, P. Geuting, P. Höschele, C. Ellersdorfer, W. Sinz, Investigation of the electro-mechanical behavior of automotive high voltage busbars under combined electrical load with varying indenter geometry and environmental conditions, J. Energy Storage 32 (2020) 101861.

[16] I. Husain, Electric and Hybrid Vehicles: Design Fundamentals, CRC Press, 2021.

[17] R.F. Sampaio, M.F. Zwicker, J.P. Pragana, I.M. Bragança, C.M. Silva, C.V. Nielsen, P.A. Martins, Busbars for e-mobility: State-of-the-art review and a new joining by forming technology, Mech. Ind. Eng.: Hist. Asp. Futur. Dir. (2021) 111–141.

[18] M. Soori, B. Arezoo, R. Dastres, Digital twin for smart manufacturing, a review, Sustain. Manuf. Serv. Econ. 2 (2023) 100017.

[19] L. Lattanzi, R. Raffaeli, M. Peruzzini, M. Pellicciari, Digital twin for smart manufacturing: A review of concepts towards a practical industrial implementation, Int. J. Comput. Integr. Manuf. 34 (6) (2021) 567–597.

[20] C. Schwarz, Z. Wang, The role of digital twins in connected and automated vehicles, IEEE Intell. Transp. Syst. Mag. 14 (6) (2022) 41–51.

[21] D. Piromalis, A. Kantaros, Digital twins in the automotive industry: The road toward physical-digital convergence, Appl. Syst. Innov. 5 (4) (2022) 65.

[22] A.M. Muslu, V. Smet, Y. Joshi, Multi-physics modeling of a power electronics package with integrated cooling, in: 2021 27th International Workshop on Thermal Investigations of ICs and Systems, THERMINIC, IEEE, 2021, pp. 1–6.

[23] C. Ling, L. Wang, C.-D. Kan, C. Yang, Thermal–electrical–mechanical coupled finite element models for battery electric vehicle, Machines 12 (9) (2024) 596.

[24] O. Tayyara, Multi-Scale Thermal Design and Optimization of High-Power Converters for Electric Vehicle Fast Chargers (Ph.D. thesis), University of Toronto (Canada), 2022.

[25] R. Torchio, F. Conte, A. Martin, N. Bianchi, M. De Soricellis, F. Toso, F. Pase, M. Scarpa, M. Filippini, M. Lurtz, et al., Design and experimental validation of a multiphysics twin of a high voltage EV motor, IEEE Trans. Transp. Electrification (2024).

[26] K. Kim, J.-I. Choi, Effect of cell-to-cell variation and module configuration on the performance of lithium-ion battery systems, Appl. Energy 352 (2023) 121888.

[27] A. Fill, T. Mader, T. Schmidt, A. Avdyli, M. Kopp, K.P. Birke, Experimental investigations on current and temperature imbalances among parallel-connected lithium-ion cells at different thermal conditions, J. Energy Storage 51 (2022) 104325.

[28] N. Saber, C.P. Richter, R. Unnthorsson, Review of thermal management techniques for prismatic Li-ion batteries, Energies 18 (3) (2025) 492.

[29] A. Venugopal, F. Robert, Laminated busbar optimization concerning physical aspects, materials, and structural modifications, in: 2022 International Conference on Power, Energy, Control and Transmission Systems, ICPECTS, IEEE, 2022, pp. 1–5.

[30] L. Radomsky, R. Keilmann, D. Ferch, R. Mallwitz, Challenges and opportunities in power electronics design for all-and hybrid-electric aircraft: a qualitative review and outlook, CEAS Aeronaut. J. 15 (4) (2024) 751–764.

[31] Y. Zhao, Y. Luo, Y. Lu, Y. He, X. Guo, S. Wang, H. Cui, Y. Zhang, Z. Wang, Effect of welding parameters on the microstructures and mechanical properties of double-pass aluminum/magnesium dissimilar metal friction stir lap welding joint, Mater. Today Commun. 26 (2021) 102132.

[32] C.-H. Lin, W.-C. Huang, Y.-C. Ke, J.-M. Song, Electrochemical analysis of surface oxide layers of various copper films in microelectronics, in: 2021 IEEE CPMT Symposium Japan, ICSJ, IEEE, 2021, pp. 61–64.

[33] K. Kamli, Z. Hadef, B. Chouial, B. Hadjoudja, Thickness effect on electrical properties of copper oxide thin films, Surf. Eng. 35 (1) (2019) 86–90.

[34] S. Ramachandran, A. Lakshminarayanan, An insight into microstructural heterogeneities formation between weld subregions of laser welded copper to stainless steel joints, Trans. Nonferr. Met. Soc. China 30 (3) (2020) 727–745.

[35] A. Venugopal, F. Robert, Impact of dimensions, apertures and terminals on stray inductance of the laminated busbar, Period. Polytech. Electr. Eng. Comput. Sci. 67 (1) (2023) 83–94.